

Transcriptome analysis reveals key genes modulated by ALK5 inhibition in a bleomycin model of systemic sclerosis

Benjamin E. Decato^{1*}, Ron Ammar^{1*}, Lauren Reinke-Breen^{1*}, John R. Thompson¹, Anthony V. Azzara^{1,2}

*These authors contributed equally.

¹Research & Early Development, Bristol-Myers Squibb Company. Route 206 & Province Line Rd, Lawrenceville, NJ 08543 USA.

²Address correspondence to Anthony V. Azzara, Ph.D.

E-mail: anthony.azzara@bms.com.

Postal address: Anthony V. Azzara, Mail Stop M.4880G, 3551 Lawrenceville Road, Princeton, NJ 08540

Running Head

Gene expression profiling of bleomycin-induced model of systemic sclerosis

Abstract

Objective: Systemic sclerosis (SSc) is a rheumatic autoimmune disease affecting roughly 20,000 people worldwide and characterized by excessive collagen accumulation in the skin and internal organs. Despite the high morbidity and mortality associated with SSc, there are no approved disease-modifying agents. Our objective in this study was to explore transcriptomic and model-based drug discovery approaches for systemic sclerosis.

Methods: In this study, we explored the molecular basis for SSc pathogenesis in a well-studied mouse model of scleroderma. We profiled the skin and lung transcriptomes of mice at multiple timepoints, analyzing the differential gene expression that underscores the development and resolution of bleomycin-induced fibrosis.

Results: We observed shared expression signatures of upregulation and downregulation in fibrotic skin and lung tissue, and observed significant upregulation of

1
2
3 key pro-fibrotic genes including *GDF15*, *Saa3*, *Cxcl10*, *Spp1*, and *Timp1*. To identify
4 changes in gene expression in responses to anti-fibrotic therapy, we assessed the
5 effect of TGF- β pathway inhibition via oral ALK5 (TGF- β receptor I) inhibitor SB525334
6 and observed a time-lagged response in the lung relative to skin. We also implemented
7 a machine learning algorithm that showed promise at predicting lung function using
8 transcriptome data from both skin and lung biopsies.
9

10
11
12 **Conclusion:** This study provides the most comprehensive look at the gene expression
13 dynamics of an animal model of systemic sclerosis to date, provides a rich dataset for
14 future comparative fibrotic disease research, and helps refine our understanding of
15 pathways at work during SSc pathogenesis and intervention.
16

17
18 **Keywords:** Systemic sclerosis, scleroderma; RNA-seq; Fibrosis; Bleomycin; ALK5
19 inhibitor
20

21 22 **Key messages**

23
24 Subcutaneous bleomycin injections induced coordinated pro-fibrotic gene expression
25 changes in skin and lung tissue.
26

27
28 Transcriptomic response to ALK5 inhibition was robust but time-lagged in lung relative
29 to skin.
30

31
32 Transcriptomic profiling from the skin and lung accurately predicted markers of lung
33 function.
34

35 36 37 **Introduction**

38
39 Systemic sclerosis (SSc, the systemic form of scleroderma) is a chronic progressive
40 disease characterized by three main features: vascular injury, immunological
41 abnormalities, and fibrosis of the skin and various internal organs, including the lung.
42

43
44 While skin fibrosis is the hallmark feature of SSc, scleroderma interstitial lung fibrosis is
45 responsible for much of the morbidity and mortality associated with this disease.(1) As
46 of 2018, an estimated 19,390 people were living with SSc with significant predicted
47 growth in new cases through 2038.(2) SSc patients with significant internal organ
48
49
50
51
52
53
54
55
56
57
58
59
60

1
2
3 involvement have a 10-year survival rate of only 38%.(3) The mechanism underlying the
4 development of fibrosis remains unclear, and current therapeutic options are limited and
5 provide only a modest benefit to patients.(4, 5)
6
7

8
9
10 A well-characterized mouse model of scleroderma involves daily subcutaneous
11 injections of the antitumor antibiotic bleomycin (BLM), which leads to localized dermal
12 fibrosis as well as pulmonary fibrosis.(6) In the present study, we utilized this model,
13 which mimics several key features of human SSc, to examine the pathological
14 mechanisms underlying the development and resolution of fibrosis in SSc. It is well
15 established that the TGF- β signaling pathway is required for bleomycin-induced fibrosis
16 in this model and that genetic or pharmacological inhibition of this pathway causes
17 resolution of dermal and pulmonary fibrosis.(7) Thus, we also used the ALK5 (TGF- β
18 receptor I) inhibitor SB525334 to investigate genome-wide changes that occur during
19 TGF- β inhibitor-mediated resolution.
20
21
22
23
24
25
26
27
28
29
30
31
32
33
34

35 We characterized the development of dermal and pulmonary fibrosis in the bleomycin-
36 induced mouse model of scleroderma. We compared skin and lung signatures, noting
37 significant overlap between the time-course trajectories of increased and decreased
38 expression, as well as produced a proof-of-concept model for predicting lung function
39 outcomes from lung and skin gene expression data, and report the expression changes
40 in well-known collagen formation and degradation genes in response to the ALK5
41 inhibitor. Taken together, the data generated in this study and our results provide a
42 trove of resources from which the scientific community can build to better understand
43 the development, progression, and treatment of scleroderma.
44
45
46
47
48
49
50
51
52
53
54
55
56
57
58
59
60

Results

Experimental design and phenotypic profiling of a bleomycin-induced mouse model of scleroderma

To induce skin and lung fibrosis, female C57BL/6NTac mice were subjected to daily subcutaneous injections of either bleomycin or PBS five times per week for two weeks. Mice were sacrificed on days 7, 14, 21, 28, or 42 following the first bleomycin injections (Figure 1). For the mice that were sacrificed on days 21 or 28 (Groups #5-10), oral dosing of the ALK5 inhibitor SB525334 was initiated one day after the last bleomycin injection. BID dosing in these groups continued through the day prior to sacrifice. To assess the extent of fibrosis, hydroxyproline analysis was conducted on skin and lung tissues from animals sacrificed at all timepoints. Additionally, flexiVent lung function analysis was performed on mice that were sacrificed on Day 21, 28, or 42 (see Methods for details).

Bleomycin induced an increase in collagen deposition in the skin and lungs, indicated by increased hydroxyproline content in both tissues (Figure 2A, B). Skin fibrosis was most prominent at days 14 and 21 and showed evidence of resolution at day 42 (Figure 2A). Treatment with the ALK5 inhibitor caused a decrease in skin fibrosis at day 21. Lung fibrosis was evident at Day 21 and peaked at day 28 (Figure 2B). Treatment with the ALK5 inhibitor caused a decrease in lung fibrosis at Days 21 and 28. Results from flexiVent analysis indicate that lung function was significantly impaired at days 21 and 28 (Figure 2C). Treatment with the ALK5 inhibitor promoted a modest improvement in lung function at both time points. Representative histopathology images at each stage

1
2
3 of the experiment for lung and skin are available in Supplementary Figure S1, available
4 at *Rheumatology* online.
5
6

7
8 RNA was isolated from skin and lung tissue harvested from mice that were sacrificed at
9 all timepoints, and bulk RNA-seq was conducted on all samples. The resulting gene
10 expression libraries allowed us to investigate transcriptional changes underlying the
11 development and regression of bleomycin-induced fibrosis, as well as the effects of
12 TGF- β pathway inhibition on both tissues. Dimensionality reduction via t-SNE(8)
13 revealed stronger separation of gene expression profiles by tissue type than by
14 timepoint, bleomycin/PBS treatment, or ALK5 intervention (Supplementary Figure S2A,
15 available at *Rheumatology* online). Principal components analysis of individual tissues
16 showed substantial variation by treatment and tissue in the first two principal
17 components for both tissues (Supplementary figure S2B, available at *Rheumatology*
18 online).
19
20
21
22
23
24
25
26
27
28
29
30
31
32
33
34

35 **Coordinated skin and lung gene expression changes in response to** 36 **bleomycin injury** 37 38 39 40

41 We first sought to understand the transcriptional changes underlying bleomycin-induced
42 fibrosis. For each of the five timepoints (days 7, 14, 21, 28, and 42), we compared PBS-
43 and bleomycin- treated mice, and summarized the number of differentially expressed
44 genes identified by limma(9) for each tissue in Figure 3A. The number of differentially
45 expressed genes increased from day 7 to a maximum at day 14, just after cessation of
46 the bleomycin treatment, and we observed substantial reduction from that maximum by
47 day 42. This pattern of differential gene expression gave us confidence that the
48
49
50
51
52
53
54
55
56
57
58
59
60

1
2
3 observed changes were driven primarily by the bleomycin treatment. For each of these
4 differentially expressed gene sets, we used GSEA to compute enrichment of pathways
5 in MSigDB including KEGG, Biocarta, and Reactome (Supplementary Figures S3 & S4,
6 available at *Rheumatology* online). We observed significant upregulation of cell cycle,
7 KEGG disease, and biosynthesis pathways through early timepoints, giving way to
8 upregulated extracellular matrix formation and degradation pathways in both tissues at
9 days 28 and 42.
10
11
12
13
14
15
16
17
18
19

20 A key objective of our study was to assess the degree and temporal trajectory of
21 change in the transcriptional profiles in skin versus lung. To do this, we performed
22 unsupervised clustering on the differentially expressed genes and explored whether
23 gene expression changes were occurring in the same direction over time for both skin
24 and lung. The clusters that resulted are shown in Figure 3B. In skin, these clusters
25 roughly represented four unique trajectories, which we have named Skin1 – Skin4:
26 persistent upregulation in response to bleomycin, followed by downregulation post-bleo
27 (Skin1); increasing downregulation in response to bleomycin, followed by upregulation
28 post-bleo (Skin2); persistent downregulation in response to bleomycin, followed by
29 upregulation post-bleo (Skin3); and increasing upregulation in response to bleomycin,
30 followed by downregulation post-bleo (Skin4).
31
32
33
34
35
36
37
38
39
40
41
42
43
44
45

46 Lung clusters were produced and named arbitrarily, and then re-ordered in Figure 3B
47 according to their closest matching Skin cluster as identified in the UpSet plot in Figure
48 3C. The largest overlap occurred between Skin1 and Lung3, meaning that most genes
49 with a persistent upregulation in response to bleomycin followed by down-regulation
50 post-bleo shared that pattern in both lung and skin. Lung cluster trajectories matched
51
52
53
54
55
56
57
58
59
60

1
2
3 skin cluster trajectories in all four cases, indicating that similar sets of genes are being
4
5 activated or repressed in response to bleomycin in both tissues. A full list of cluster
6
7 membership is available in Supplementary Table S1 (available at *Rheumatology*
8
9 online), and cluster probability distributions are shown in Supplementary Figure S5B
10
11 (available at *Rheumatology* online).
12
13
14

15
16 To get a more detailed view of which genes showed the largest coordinated bleomycin-
17
18 induced changes in both skin and lung, we generated volcano plots of differential
19
20 expression for skin and lung at day 14, when bleo-induced changes reached an apex in
21
22 both tissues (Figure 3D). We observed 261 and 59 genes that displayed differential
23
24 expression between bleomycin and PBS in skin and lung, respectively (colored blue,
25
26 absolute log fold change > 3 and FDR-corrected p-value < 0.1; Supplemental Table S2,
27
28 available at *Rheumatology* online). Exploration of overlap yielded 8 genes differentially
29
30 expressed in both tissues (labeled on both volcano plots; Timp1 log fold change 2.913
31
32 in skin). This provided us with a short list of large, coordinated gene expression
33
34 changes across both tissues. Notably, many of these genes have been previously
35
36 shown to be increased in SSc patients (see Discussion for a complete list). Taken
37
38 together, these results point to shared pathophysiology between the bleomycin-induced
39
40 mouse model of scleroderma and human SSc.
41
42
43
44
45

46 **Time-lagged differential gene expression of *ALK5* inhibitor driven** 47 48 **intervention** 49 50

51
52
53 Next, we sought to understand the effect of the *ALK5* inhibitor SB525334 on resolution
54
55 of bleomycin-induced fibrosis by exploring differential expression between SB525334-
56
57
58
59
60

1
2
3 treated and vehicle-treated mice in both lung and skin at days 21 and 28. Figure 4A
4 shows that at day 21, there are substantial expression differences in the SB525334-
5 treated mice in skin, but no subsequent changes in lung. By day 28, a comparable
6 number of differentially expressed genes are observable in both tissues, suggesting that
7 systemic effects of oral SB525334 may not be temporally consistent across tissues.
8
9

10
11
12 Of the genes showing differential expression in mice treated with SB525334, 1,055
13 were differential at both timepoints in the skin, and 750 were shared between skin and
14 lung on day 28 (Figure 4B). Analysis of the top differentially expressed genes at Day 28
15 between SB525334 and vehicle treated samples revealed downregulation of several
16 keratin associated genes in skin and one, *Krt4*, in lung (Figure 4C). Several collagen
17 genes including *Col1a1*, *Col1a2*, *Col3a1*, *Col5a1*, *Col5a2*, and *Col12a1* also displayed
18 time-lagged differential expression between bleomycin- and PBS treated mice, and
19 reductions in response to SB525334 (Supplemental Figure S6, available at
20
21
22 *Rheumatology* online). GSEA pathway analysis (see Methods) for genes significantly
23 differentially expressed in skin and lung at day 28 revealed downregulation of the Naba
24 collagen pathway in SB525334-treated skin but not lung, suggesting a potential for
25 continued lag in response (Figure 4D). One gene, *Bgn*, codes for biglycan and was
26 significantly downregulated in the SB525334 group in all four tissues/timepoints pairs.
27 Biglycan has been previously associated with type I and type II collagens(10), and its
28 synthesis is stimulated by *ALK5*.(11)
29
30
31
32
33
34
35
36
37
38
39
40
41
42
43
44
45
46
47
48
49
50

51 **Predicting lung function with lung and skin transcriptional profiles**

52
53
54
55
56
57
58
59
60

1
2
3 Of the measurements available for mouse lung function, inspiratory capacity (IC) is
4 considered to be the most analogous to forced vital capacity (FVC). In general, we
5 observed that IC was higher for PBS-treated mice than for bleomycin-treated mice,
6 indicating that bleomycin treatment caused impairment of lung function.
7

8
9
10 Trained on the lung and skin transcriptional data, we constructed models of IC (see
11 Methods) in order to determine if lung or skin biopsies could function as surrogate
12 biomarkers of lung function. Due to limited availability of validation data sets, we used
13 repeated cross-validated performance to assess the models.
14

15 We observed that $\mathcal{M}_{\text{lung}}$ and $\mathcal{M}_{\text{skin}}$ models were equally informative for predicting IC
16 ($\text{AUROC}(\text{IC}_{\text{lung}}) \approx 0.8$ and $\text{AUROC}(\text{IC}_{\text{skin}}) \approx 0.8$; Figure 5). While our sample
17 numbers were limited, these results are encouraging and suggest that RNA-seq from
18 lung or skin could serve as a biomarker of lung function.
19
20
21
22
23
24
25
26
27
28
29
30
31
32
33

34 Discussion

35
36
37
38 The subcutaneous bleomycin mouse model is widely used to support efforts to develop
39 novel therapies for scleroderma, including *in vivo* efficacy studies and biomarker
40 identification and validation. The transcriptomics data presented here represents a
41 novel resource that can be utilized to support ongoing and future studies using this
42 model. The novel design of the present study allows for the comparison of gene
43 expression changes in both skin and lung in response to bleomycin. Our results
44 demonstrate a coordinated response to bleomycin across tissue types, highlighted by
45 the trajectory clusters in Figure 3B. These findings reflect one of the hallmark features
46
47
48
49
50
51
52
53
54
55
56
57
58
59
60

1
2
3 seen in SSc patients: the relatively concurrent development of fibrosis across multiple
4 organs.(12) Thus, our datasets represent a novel resource that can be used to further
5 investigate the systemic development and progression of tissue fibrosis. Further, these
6 data represent the possibility that genetic signatures from peripherally accessible skin
7 biopsies could reflect and/or predict the disease status of the lung. This may represent a
8 significant enhancement over current lung evaluations, which are limited to function
9 imaging-based morphology, due to the risk associated with taking lung tissue samples
10 or lavage.
11
12
13
14
15
16
17
18
19
20
21

22 Additionally, as highlighted in Figure 3D, a number of genes that exhibited differential
23 expression in both skin and lung in response to bleo have been shown to be increased
24 in SSc patients:
25
26
27
28
29

30 GDF15 – GDF15 (growth differentiation factor 15) is a distant member of the TGF- β
31 family. GDF15 is increased in the serum of SSc patients and is correlated with disease
32 severity and extent of organ involvement, particularly with lung fibrosis.(13, 14)
33
34
35
36
37

38 CXCL10 – CXCL10 (also known as IP-10) is a Th1 chemokine that is induced by IFN-
39 γ .(15) CXCL10 is increased in the skin and serum of SSc patients, and increased serum
40 levels of CXCL10 are associated with disease severity and increased internal organ
41 involvement.(16-18)
42
43
44
45
46
47

48 MMP10 – MMP10 (also known as stromelysin 2) is a matrix metalloproteinase that
49 plays a critical role in ECM degradation and remodeling during wound healing and
50 vascular remodeling.(19) MMP10 is increased in the serum and pulmonary arteries of
51 SSc patients with pulmonary hypertension.(20)
52
53
54
55
56
57
58
59
60

1
2
3 TIMP-1 – TIMP-1 (tissue inhibitor of matrix metalloproteinase-1) levels are increased in
4 the serum and lesional skin of SSc patients.(21-23) Interestingly, TIMP-1 is one of three
5 soluble proteins comprising the ELF (enhanced liver fibrosis) test. The ELF test was
6 recently validated as an SSc biomarker that correlates with both skin and lung
7 involvement.(24)
8
9
10
11
12
13

14
15 Saa3 – Saa3 is a member of the serum amyloid A (SAA) family, which consist of early-
16 phase proteins known to play a key role in inflammation.(25) Serum SAA levels are
17 increased in SSc patients and correlated with the extent of pulmonary involvement.(25,
18 26)
19
20
21
22
23
24

25
26 Retnla – Retnla (resistin-like alpha, also known as RELM- α or FIZZ1) has been
27 identified as an M2 macrophage marker in mice.(27) The closest human homolog,
28 RETLN- β , is increased in the lungs of SSc patients with pulmonary hypertension.(28)
29
30
31
32

33
34 SPP1 – SPP1 (secreted phosphoprotein 1, also known as osteopontin) is a matricellular
35 protein that exhibits proinflammatory and profibrotic properties.(29) Osteopontin is
36 increased in both the serum and lesional skin of SSc patients.(29, 30)
37
38
39
40

41
42 These findings support the utility of this model to help identify novel targets and/or
43 biomarkers for SSc. Our data showing that Alk5 inhibition exhibits a time-lagged
44 response in lung versus skin suggests that *in vivo* compound efficacy studies may need
45 to be designed to allow for analysis of different tissues at multiple timepoints to
46 thoroughly assess systemic treatment effects.
47
48
49
50
51
52
53
54
55
56
57
58
59
60

1
2
3 Our preliminary analyses using novel modeling techniques to predict lung function
4 based on gene expression have laid the groundwork for future translational studies. Our
5 findings suggest that there are similarities in gene expression patterns in skin and lung
6 that can be taken advantage of to allow for an increased ability to monitor the fibrotic
7 state of the lungs of SSc patients by assessing gene expression changes in skin
8 biopsies. Analysis of gene expression patterns in the skin may potentially offer insight
9 into which patients will develop SSc-ILD, an aspect of the disease that accounts for a
10 considerable proportion of its morbidity and mortality. The ability to better identify these
11 at-risk patients would allow for earlier treatment and improved patient outcomes.
12
13
14
15
16
17
18
19
20
21
22
23
24

25 **Methods**

26 **Study design**

27
28
29 Twelve-week-old female C57BL/6NTac mice (Taconic) were given daily subcutaneous
30 injections of either bleomycin (Hospira; 10 mg/kg per day) or PBS (vehicle control) in a
31 shaved interscapular region. Injections were done using a 27-gauge needle, five times
32 per week for two consecutive weeks (Days 0-4 and 7-11, inclusive). Mice were re-
33 shaved as necessary, and circles were re-drawn every 1-2 days throughout the
34 study.(31, 32)
35
36
37
38
39
40
41
42
43
44
45
46

47 Beginning on Day 12, the ALK5 inhibitor SB525334 (30mpk) or vehicle was delivered
48 (PO, BID dosing). Note that Groups 1-2 and Groups 3-4 were sacrificed on Day 7 and
49 Day 14, respectively, and thus did not receive oral dosing. Groups 5-7 were sacrificed
50 on Day 21. The last oral doses were administered on Day 27. Groups 8-10 were
51
52
53
54
55
56
57
58
59
60

1
2
3 sacrificed on Day 28. Groups 11-12 (which specifically serve to assess resolution in this
4 model, and do not examine the effect of SB525334) were sacrificed on Day 42.
5
6
7

8
9 Supplementary figure S7A (available at *Rheumatology* online) provides additional
10 information on groups (12 groups, n = 8-10 per group at onset of the study; a total of
11 seven animals died during the study).
12
13
14
15

16 **Lung function analysis**

17
18
19
20 The mechanical properties of the mouse lungs were determined using the flexiVent
21 apparatus (Scireq, Montreal, QC, Canada). In brief, mice were anesthetized by
22 intraperitoneal administration of Ketamine (91 mg/kg; VedCo) and Xylazine (9.1 mg/kg;
23 Akorn Animal Health), a tracheotomy was performed, and an 18-gauge cannula was
24 inserted into a slit in the trachea and connected to the flexiVent computer-controlled
25 rodent ventilator. After an initial period of ventilation, measurement of lung mechanical
26 properties was initiated by a computer-generated program to measure inspiratory
27 capacity, compliance, lung resistance, tissue elastance, and tissue damping. These
28 measurements were repeated 3 times for each animal.
29
30
31
32
33
34
35
36
37
38
39
40
41

42 **Analysis of hydroxyproline content**

43
44
45 Hydroxyproline analysis was conducted on half of an 8mm skin biopsy, or on the
46 middle, inferior, and post-caval lung lobes. The QuickZyme Total Collagen Assay kit
47 (QuickZyme Biosciences, The Netherlands) was used according to the manufacturer's
48 instructions. For skin, hydroxyproline levels were normalized to tissue weights to
49 account for potential variability in tissue procurement.
50
51
52
53
54
55
56
57
58
59
60

RNA-seq library preparation and pre-processing

Small pieces of tissue (~5mg) were added to a 2ml tube with one 5mm diameter stainless steel bead (Cat # 69989, Qiagen, Valencia, CA) and 1.2ml Trizol® (Life Technologies, Cat # 15596018, Grand Island, NY). Tissue was homogenized by TissueLyzerII (Qiagen, Valencia, CA) (lung for 1 minute, skin for 3 minutes). 500ul chloroform was then added to the homogenate. After vortexing for 30 seconds, samples were centrifuged at 14,000 rpm for 15 minutes at 4°C. The supernatant layer was collected into a deep 96-well plate, mixed with 50ul 70% ethanol. The mixtures were transferred to the RNeasy 96 well plate, (RNeasy® 96 Kit, Cat # 74881, Qiagen, Valencia, CA 91355). RNA was isolated by following the manufacturer's protocol. RNA was eluted in 90ul H₂O then treated with DNaseI by adding 10ul DNaseI 10X buffer + 2ul DNaseI (ThermoFisher, Cat# AM2222) for 15 min at room temperature. Treated RNA was cleaned up by using RNeasy® 96 Kit following the manufacturer's protocol. The quality and quantity of the isolated total RNA were evaluated with a NanoDrop 8000 spectrophotometer (Thermo Scientific, Wilmington, DE). RNA was then normalized to 50ng/ul, randomized with DOE, prepared using the Illumina TruSeq Total RNA-Gold kit and sequenced with Illumina HiSeq sequencing.

Raw sequence files were processed by the bcl2fastq software in BaseSpace to generate FASTQ files for each sample. Sequence reads in the FASTQ files were then aligned to the Mouse.B38 genome build using Omicsoft ArrayStudio with the OSA alignment algorithm.(33) Ensembl gene models (version R86) were used by Omicsoft's reimplementations of the RSEM algorithm to generate gene-level counts for each

1
2
3 sample.(34, 35) The resulting gene by sample count matrix was further processed in R
4
5 using voomWithQualityWeights together with a limma linear modeling workflow to
6
7 assess differential gene expression.(36-38) Quality control statistics including mapping
8
9 rate, mitochondrial DNA rate, and more are available in Supplemental table S3.
10
11

12
13 RNA quality as measured through RIN score is available in Supplementary figure S7B
14
15 (available at *Rheumatology* online). Multiple plates were used for RNA-seq library
16
17 preparation: we used ComBat(39) to correct for this confounding variable and
18
19 demonstrate the reduction of variance explained by plate pre- and post-run using
20
21 Variance Partition Analysis (Supplementary figure S7C & D, available at *Rheumatology*
22
23 online).(40)
24
25
26
27

28 **Differential gene expression analysis**

29
30
31
32 Differential expression analysis was performed independently for lung and skin samples
33
34 using limma(9) with plate and RIN score included as covariates. Genes were identified
35
36 as differentially expressed if their FDR-corrected p-value was less than 0.1; p-value
37
38 distributions are available in Supplementary figures S5A and S5C (available at
39
40 *Rheumatology* online) for all contrasts studied. All differential expression performed for
41
42 every tissue and contrast, with gene names, log fold changes, and adjusted p-values is
43
44 summarized in Supplementary Table S4 (available at *Rheumatology* online).
45
46
47
48

49 Time-course clusters were identified using TCseq(41) and UpSet plots were generated
50
51 using UpSetR.(42)
52
53
54
55
56
57
58
59
60

1
2
3 We used the Molecular Signatures Database (MSigDB)(43) and computed Gene Set
4 Enrichment Analysis as described previously.(44) We used the fast implementation
5
6 fgsea.(45)
7
8
9

10
11 The GSEA enrichment score (ES) represents the degree to which a gene set is
12 overrepresented at the top or bottom of a ranked list of genes. A positive ES indicates
13 gene set enrichment at the top of the ranked list, and a negative ES indicates gene set
14 enrichment at the bottom of the ranked list. The ES is a function of gene set size, and,
15 therefore, ESs cannot be directly compared across gene sets. Cross-gene set
16 comparisons are facilitated by the normalized enrichment score (NES).
17
18
19
20
21
22
23
24
25

26 **Model construction and optimization**

27
28 Inspiratory Capacity (IC) was modeled as a continuous response by fitting a linear
29 regression model to the RNA-Seq expression data, computed with an elastic net
30 regularization path. We modeled lung and skin tissues separately yielding two models of
31 IC, $\mathcal{M}_{\text{lung}}$ and $\mathcal{M}_{\text{skin}}$. Linear regression can be unreliable when $n < p$ (relatively few
32 samples with many transcript observations). By linearly combining both λ_1 and λ_2
33 penalties of the lasso and ridge regression methods, respectively, elastic net
34 regularization improves model performance.(46-48)
35
36
37
38
39
40
41
42
43
44

45 Elastic net training requires the selection of both a lasso and ridge mixing parameter, α ,
46 and a penalty strength parameter, λ . To identify the optimal combination with the
47 highest performance, we conducted 10-fold balanced cross-validation for each (α, λ)
48 pair in a grid search on each training set. We chose $\alpha = 0.95$ based on the suggestion
49 in the glmnet documentation to set $\alpha = 1 - \lambda$ for some small $\lambda > 0$.⁴⁶ The rationale is to
50
51
52
53
54
55
56
57
58
59
60

1
2
3 improve numerical stability and reduce the degeneracies caused by high correlations
4
5 between covariates.
6

7 We performed 100 repeats of 10-fold cross-validation in caret to select the λ that
8
9 yielded the highest performing final model (with the lowest mean-squared error).(49)
10
11
12

13 **Disclosures**

14 BED, RA, LR-B, JRT, and AVA were employees of Bristol Myers Squibb when the work
15 was done and may hold stock in the company.
16
17
18

19 **Funding Source**

20 All work described in this manuscript was funded by Bristol Myers Squibb.
21
22
23
24

25 **Ethics approval**

26
27
28
29 This study was conducted with the approval of the Bristol Myers Squibb Internal Animal
30
31 Care and Use Committee. All protocols and procedures were reviewed and approved
32
33 prior to the start of the animal experiments.
34
35
36
37

38 **Data and code availability**

39
40
41
42 All RNA-seq data analyzed in this manuscript was deposited in GEO under accession
43
44 number GSE132869. Code associated with this analysis can be found at
45
46 www.github.com/bdecat0/SSc-Transcriptome-Manuscript-Code.
47
48
49

50 **Acknowledgements**

51
52
53
54
55
56
57
58
59
60

1
2
3 The authors would like to thank L. Burns for *in vivo* support, Yan Zhang for isolating
4 RNA from skin and lung tissue, Manling Ma-Edmonds for conducting the RNA-seq
5 library prep and running the RNA-seq analysis, and anonymous reviewers for their
6 helpful feedback.
7
8
9
10
11
12
13
14

15 **Figure Captions**

16
17
18
19 **Figure 1: Overview of study design and animal groups.** Bleomycin was dosed at 10
20 mg/kg/day, and SB525334 was dosed at 30 mg/kg. BLM: bleomycin, BID: Twice a day;
21 PO: Oral administration; SC: subcutaneous
22
23
24
25

26
27 **Figure 2: Effects of bleomycin treatment and ALK5 inhibition on markers of**
28 **collagen formation and lung function.** (A) Hydroxyproline content of skin tissue. (B)
29 Hydroxyproline content of lung tissue (ml, middle lobe; il, inferior lobe; pcl, postcaval
30 lobe). (C) Lung function as assessed by flexiVent analysis. (BLM, bleomycin; ALK5i, the
31 ALK5 inhibitor SB525334). Error bars represent SEM. Statistical significance was
32 assessed using One-way ANOVA with Bonferroni's correction.
33
34
35
36
37
38
39
40

41
42 **Figure 3: Integrative differential gene expression analysis between bleomycin-**
43 **treated mice and control across tissues.** (A) Number of differentially expressed
44 genes in lung and skin between bleomycin (BLM) and PBS treated mice. (B) Cluster-
45 matched patterns of z-score normalized differential expression in skin (top) and skin
46 (bottom). (C) UpSet plot showing the number of genes in each cluster (left) and
47 magnitude of overlaps between clusters (top). (D) Volcano plots of differential
48
49
50
51
52
53
54
55
56
57
58
59
60

1
2
3 expression in skin and lung, colored by FDR-corrected significance in skin and an
4
5 absolute log-fold-change ≥ 3 , with shared genes labeled on the lung volcano plot.
6
7

8
9 **Figure 4: Differential gene expression and pathway enrichment in response to**
10 **ALK5i treatment.** (A) Number of differentially expressed genes in lung and skin
11 between *ALK5* inhibitor treated and PBS treated mice. (B) UpSet plot showing the
12 overlap of differentially expressed gene sets in the four time/tissue pairs for *ALK5*
13 inhibitor vs PBS treated mice. (C) Pathway enrichment UpDown plots showing the
14 fraction and number of genes in each pathway upregulated/downregulated in the
15 SB525334 arm compared to vehicle on day 28 for skin and lung.
16
17
18
19
20
21
22
23
24
25

26 **Figure 5: Boxplots of R^2 predictive power for elastic net models predicting inspiratory**
27 **capacity from expression data.**
28
29
30

31 References

- 32
33
34
35
36 1. Simeon C, Armadans L, Fonollosa V, Solans R, Selva A, Villar M, et al. Mortality and
37 prognostic factors in Spanish patients with systemic sclerosis. *Rheumatology*. 2003;42(1):71-5.
38 2. Royle JG, Lanyon PC, Grainge MJ, Abhishek A, Pearce FA. The incidence, prevalence,
39 and survival of systemic sclerosis in the UK Clinical Practice Research Datalink. *Clinical*
40 *rheumatology*. 2018;37(8):2103-11.
41 3. Korman BD, Criswell LA. Recent advances in the genetics of systemic sclerosis: toward
42 biological and clinical significance. *Current rheumatology reports*. 2015;17(3):1-11.
43 4. Distler JH, Feghali-Bostwick C, Soare A, Asano Y, Distler O, Abraham DJ. Frontiers of
44 antifibrotic therapy in systemic sclerosis. *Arthritis & rheumatology*. 2017;69(2):257-67.
45 5. Volkmann ER, Varga J. Emerging targets of disease-modifying therapy for systemic
46 sclerosis. *Nature Reviews Rheumatology*. 2019;15(4):208-24.
47 6. Błyszczuk P, Kozlova A, Guo Z, Kania G, Distler O. Experimental Mouse Model of
48 Bleomycin-Induced Skin Fibrosis. *Current protocols in immunology*. 2019;126(1):e88.
49 7. Meng X-m, Nikolic-Paterson DJ, Lan HY. TGF- β : the master regulator of fibrosis. *Nature*
50 *Reviews Nephrology*. 2016;12(6):325.
51 8. Van der Maaten L, Hinton G. Visualizing data using t-SNE. *Journal of machine learning*
52 *research*. 2008;9(11).
53 9. Ritchie ME, Phipson B, Wu D, Hu Y, Law CW, Shi W, et al. limma powers differential
54 expression analyses for RNA-sequencing and microarray studies. *Nucleic acids research*.
55 2015;43(7):e47-e.
56
57
58
59
60

10. Schön herr E, Witsch-Prehm P, Harrach B, Robenek H, Rauterberg J, Kresse H. Interaction of biglycan with type I collagen. *Journal of Biological Chemistry*. 1995;270(6):2776-83.
11. Burch ML, Yang SN, Ballinger ML, Getachew R, Osman N, Little PJ. TGF- β stimulates biglycan synthesis via p38 and ERK phosphorylation of the linker region of Smad2. *Cellular and Molecular Life Sciences*. 2010;67(12):2077-90.
12. Asano Y, Varga J, editors. Rationally-based therapeutic disease modification in systemic sclerosis: Novel strategies. *Seminars in cell & developmental biology*; 2020: Elsevier.
13. Yanaba K, Asano Y, Tada Y, Sugaya M, Kadono T, Sato S. Clinical significance of serum growth differentiation factor-15 levels in systemic sclerosis: association with disease severity. *Modern rheumatology*. 2012;22(5):668-75.
14. Lambrecht S, Smith V, De Wilde K, Coudenys J, Decuman S, Deforce D, et al. Growth differentiation factor 15, a marker of lung involvement in systemic sclerosis, is involved in fibrosis development but is not indispensable for fibrosis development. *Arthritis & Rheumatology*. 2014;66(2):418-27.
15. Crescioli C, Corinaldesi C, Riccieri V, Raparelli V, Vasile M, Del Galdo F, et al. Association of circulating CXCL10 and CXCL11 with systemic sclerosis. *Annals of the rheumatic diseases*. 2018;77(12):1845-6.
16. Antonelli A, Ferri C, Fallahi P, Ferrari SM, Giuggioli D, Colaci M, et al. CXCL10 (α) and CCL2 (β) chemokines in systemic sclerosis—a longitudinal study. *Rheumatology*. 2008;47(1):45-9.
17. Rabquer BJ, Tsou P-S, Hou Y, Thirunavukkarasu E, Haines GK, Impens AJ, et al. Dysregulated expression of MIG/CXCL9, IP-10/CXCL10 and CXCL16 and their receptors in systemic sclerosis. *Arthritis research & therapy*. 2011;13(1):1-10.
18. Liu X, Mayes MD, Tan FK, Wu M, Reveille JD, Harper BE, et al. Correlation of interferon-inducible chemokine plasma levels with disease severity in systemic sclerosis. *Arthritis & Rheumatism*. 2013;65(1):226-35.
19. Sokai A, Handa T, Tanizawa K, Oga T, Uno K, Tsuruyama T, et al. Matrix metalloproteinase-10: a novel biomarker for idiopathic pulmonary fibrosis. *Respiratory research*. 2015;16(1):1-8.
20. Avouac J, Guignabert C, Hoffmann-Vold AM, Ruiz B, Dorfmüller P, Pezet S, et al. Role of stromelysin 2 (matrix metalloproteinase 10) as a novel mediator of vascular remodeling underlying pulmonary hypertension associated with systemic sclerosis. *Arthritis & Rheumatology*. 2017;69(11):2209-21.
21. Young-Min S, Beeton C, Loughton R, Plumpton T, Bartram S, Murphy G, et al. Serum TIMP-1, TIMP-2, and MMP-1 in patients with systemic sclerosis, primary Raynaud's phenomenon, and in normal controls. *Annals of the rheumatic diseases*. 2001;60(9):846-51.
22. Meng C, Chen Xe, Li J, Wu Y, Liu H. Expression of MMP-9 and TIMP-1 in lesions of systemic sclerosis and its implications. *Journal of Huazhong University of Science and Technology [Medical Sciences]*. 2008;28(4):480-2.
23. Kuźnik-Trocha K, Winsz-Szczotka K, Komosińska-Vassev K, Jura-Półtorak A, Kotulska-Kucharz A, Kucharz EJ, et al. Plasma glycosaminoglycan profiles in systemic sclerosis: associations with MMP-3, MMP-10, TIMP-1, TIMP-2, and TGF-beta. *BioMed research international*. 2020;2020.
24. Abignano G, Blagojevic J, Bissell L-A, Dumitru RB, Eng S, Allanore Y, et al. European multicentre study validates enhanced liver fibrosis test as biomarker of fibrosis in systemic sclerosis. *Rheumatology*. 2019;58(2):254-9.
25. Lakota K, Carns M, Podluszky S, Mrak-Poljsak K, Hinchcliff M, Lee J, et al. Serum amyloid A is a marker for pulmonary involvement in systemic sclerosis. *PloS one*. 2015;10(1):e0110820.

26. Lis-Święty A, Widuchowska M, Brzezińska-Wcisło L, Kucharz E. High acute phase protein levels correlate with pulmonary and skin involvement in patients with diffuse systemic sclerosis. *Journal of International Medical Research*. 2018;46(4):1634-9.
27. Manetti M. Deciphering the alternatively activated (M2) phenotype of macrophages in scleroderma. *Experimental dermatology*. 2015;24(8):576-8.
28. Angelini DJ, Su Q, Yamaji-Kegan K, Fan C, Teng X, Hassoun PM, et al. Resistin-like molecule- β in scleroderma-associated pulmonary hypertension. *American journal of respiratory cell and molecular biology*. 2009;41(5):553-61.
29. Wu M, Schneider DJ, Mayes MD, Assassi S, Arnett FC, Tan FK, et al. Osteopontin in systemic sclerosis and its role in dermal fibrosis. *Journal of Investigative Dermatology*. 2012;132(6):1605-14.
30. Corallo C, Volpi N, Franci D, Montella A, Biagioli M, Mariotti G, et al. Is osteopontin involved in cutaneous fibroblast activation? Its hypothetical role in scleroderma pathogenesis. *International journal of immunopathology and pharmacology*. 2014;27(1):97-102.
31. Bhattacharyya S, Tamaki Z, Wang W, Hinchcliff M, Hoover P, Getsios S, et al. FibronectinEDA promotes chronic cutaneous fibrosis through Toll-like receptor signaling. *Science translational medicine*. 2014;6(232):232ra50-ra50.
32. Huang J, Beyer C, Palumbo-Zerr K, Zhang Y, Ramming A, Distler A, et al. Nintedanib inhibits fibroblast activation and ameliorates fibrosis in preclinical models of systemic sclerosis. *Annals of the rheumatic diseases*. 2016;75(5):883-90.
33. Hu J, Ge H, Newman M, Liu K. OSA: a fast and accurate alignment tool for RNA-Seq. *Bioinformatics*. 2012;28(14):1933-4.
34. Li J, Hu J, Newman M, Liu K, Ge H. RNA-seq analysis pipeline based on oshell environment. *IEEE/ACM transactions on computational biology and bioinformatics*. 2014;11(5):973-8.
35. Li B, Ruotti V, Stewart RM, Thomson JA, Dewey CN. RNA-Seq gene expression estimation with read mapping uncertainty. *Bioinformatics*. 2010;26(4):493-500.
36. Law CW, Chen Y, Shi W, Smyth GK. voom: Precision weights unlock linear model analysis tools for RNA-seq read counts. *Genome biology*. 2014;15(2):1-17.
37. Liu R, Holik AZ, Su S, Jansz N, Chen K, Leong HS, et al. Why weight? Modelling sample and observational level variability improves power in RNA-seq analyses. *Nucleic acids research*. 2015;43(15):e97-e.
38. Law CW, Alhamdoosh M, Su S, Dong X, Tian L, Smyth GK, et al. RNA-seq analysis is easy as 1-2-3 with limma, Glimma and edgeR. *F1000Research*. 2016;5.
39. Leek JT, Johnson WE, Parker HS, Jaffe AE, Storey JD. The sva package for removing batch effects and other unwanted variation in high-throughput experiments. *Bioinformatics*. 2012;28(6):882-3.
40. Hoffman GE, Schadt EE. variancePartition: interpreting drivers of variation in complex gene expression studies. *BMC bioinformatics*. 2016;17(1):1-13.
41. Wu M GL. TCseq: Time course sequencing data analysis. 2020;R package version 1.14.0.
42. Conway JR, Lex A, Gehlenborg N. UpSetR: an R package for the visualization of intersecting sets and their properties. *Bioinformatics*. 2017;33(18):2938-40.
43. Liberzon A, Birger C, Thorvaldsdóttir H, Ghandi M, Mesirov JP, Tamayo P. The molecular signatures database hallmark gene set collection. *Cell systems*. 2015;1(6):417-25.
44. Subramanian A, Tamayo P, Mootha VK, Mukherjee S, Ebert BL, Gillette MA, et al. Gene set enrichment analysis: a knowledge-based approach for interpreting genome-wide expression profiles. *Proceedings of the National Academy of Sciences*. 2005;102(43):15545-50.
45. Sergushichev AA. An algorithm for fast preranked gene set enrichment analysis using cumulative statistic calculation. *BioRxiv*. 2016:060012.

- 1
- 2
- 3
- 4 46. Zou H, Hastie T. Regularization and variable selection via the elastic net. *Journal of the*
- 5 *royal statistical society: series B (statistical methodology)*. 2005;67(2):301-20.
- 6 47. Friedman J, Hastie T, Tibshirani R. Regularization paths for generalized linear models
- 7 *via coordinate descent*. *Journal of statistical software*. 2010;33(1):1.
- 8 48. James G, Witten D, Hastie T, Tibshirani R. *An introduction to statistical learning (Vol.*
- 9 *112, p. 18)*. New York: springer; 2013.
- 10 49. Kuhn M. Building predictive models in R using the caret package. *J Stat Softw*.
- 11 *2008;28(5):1-26*.
- 12
- 13
- 14
- 15
- 16
- 17
- 18
- 19
- 20
- 21
- 22
- 23
- 24
- 25
- 26
- 27
- 28
- 29
- 30
- 31
- 32
- 33
- 34
- 35
- 36
- 37
- 38
- 39
- 40
- 41
- 42
- 43
- 44
- 45
- 46
- 47
- 48
- 49
- 50
- 51
- 52
- 53
- 54
- 55
- 56
- 57
- 58
- 59
- 60

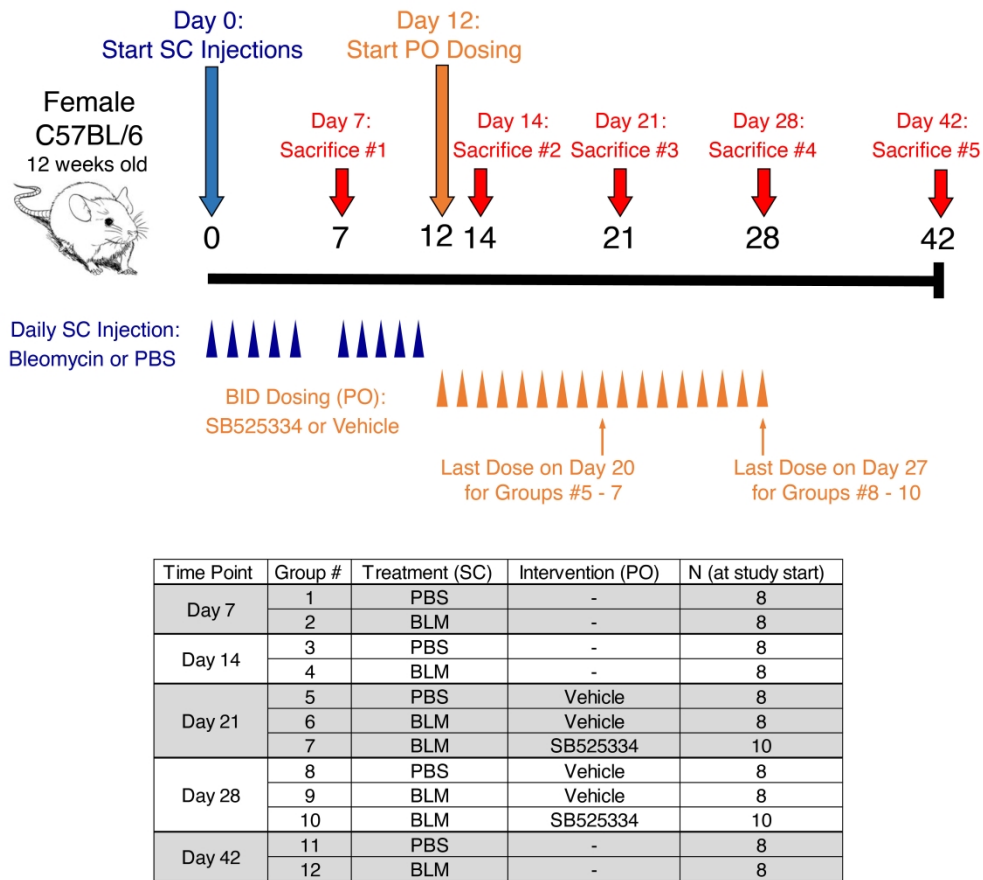


Figure 1: Overview of study design and animal groups. Bleomycin was dosed at 10 mg/kg/day, and SB525334 was dosed at 30 mg/kg. (BLM, bleomycin)

203x190mm (600 x 600 DPI)

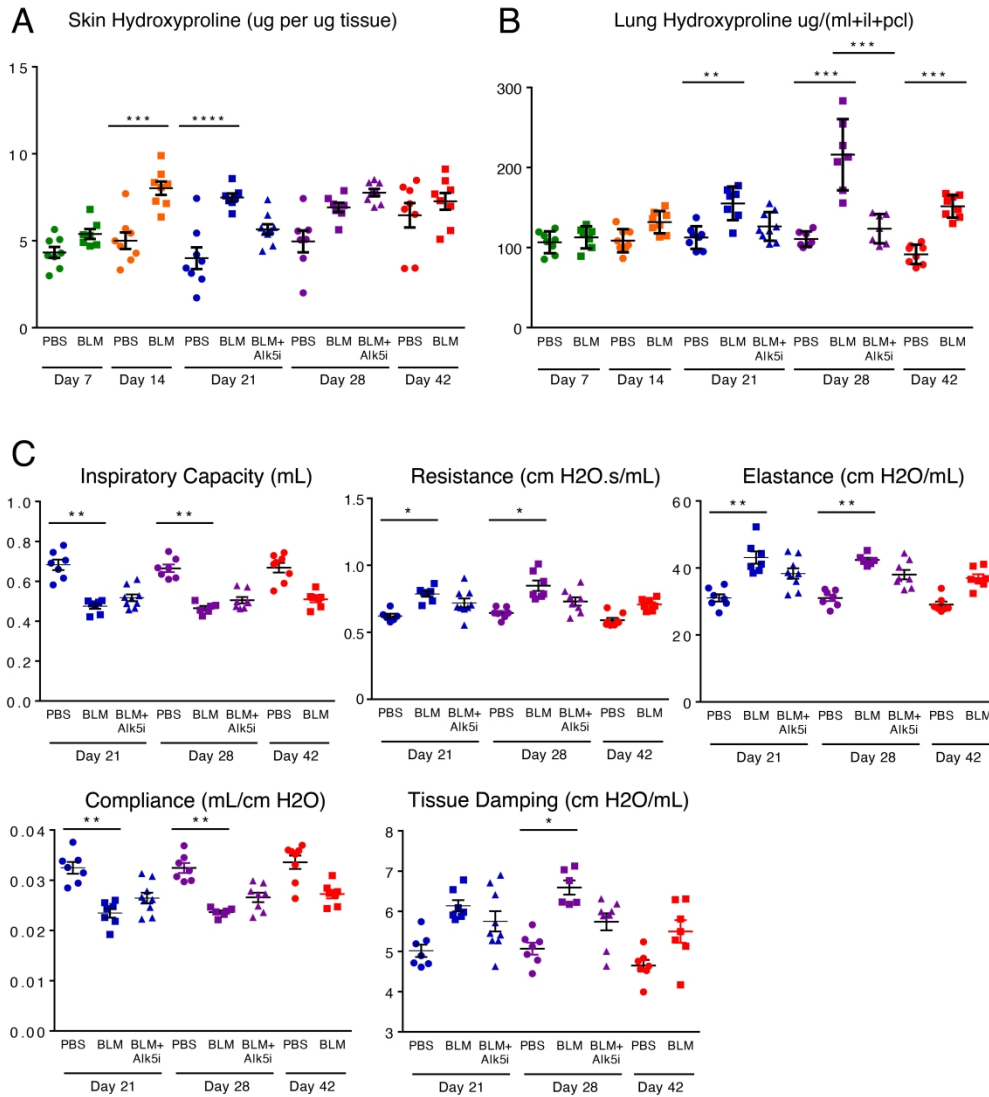


Figure 2: (A) Hydroxyproline content of skin tissue. (B) Hydroxyproline content of lung tissue (ml, middle lobe; il, inferior lobe; pcl, postcaval lobe). (C) Lung function as assessed by flexiVent analysis. (BLM, bleomycin; ALK5i, the ALK5 inhibitor SB525334). Error bars represent SEM. Statistical significance was assessed using One-way ANOVA with Bonferroni's correction.

203x228mm (600 x 600 DPI)

1
2
3
4
5
6
7
8
9
10
11
12
13
14
15
16
17
18
19
20
21
22
23
24
25
26
27
28
29
30
31
32
33
34
35
36
37
38
39
40
41
42
43
44
45
46
47
48
49
50
51
52
53
54
55
56
57
58
59
60

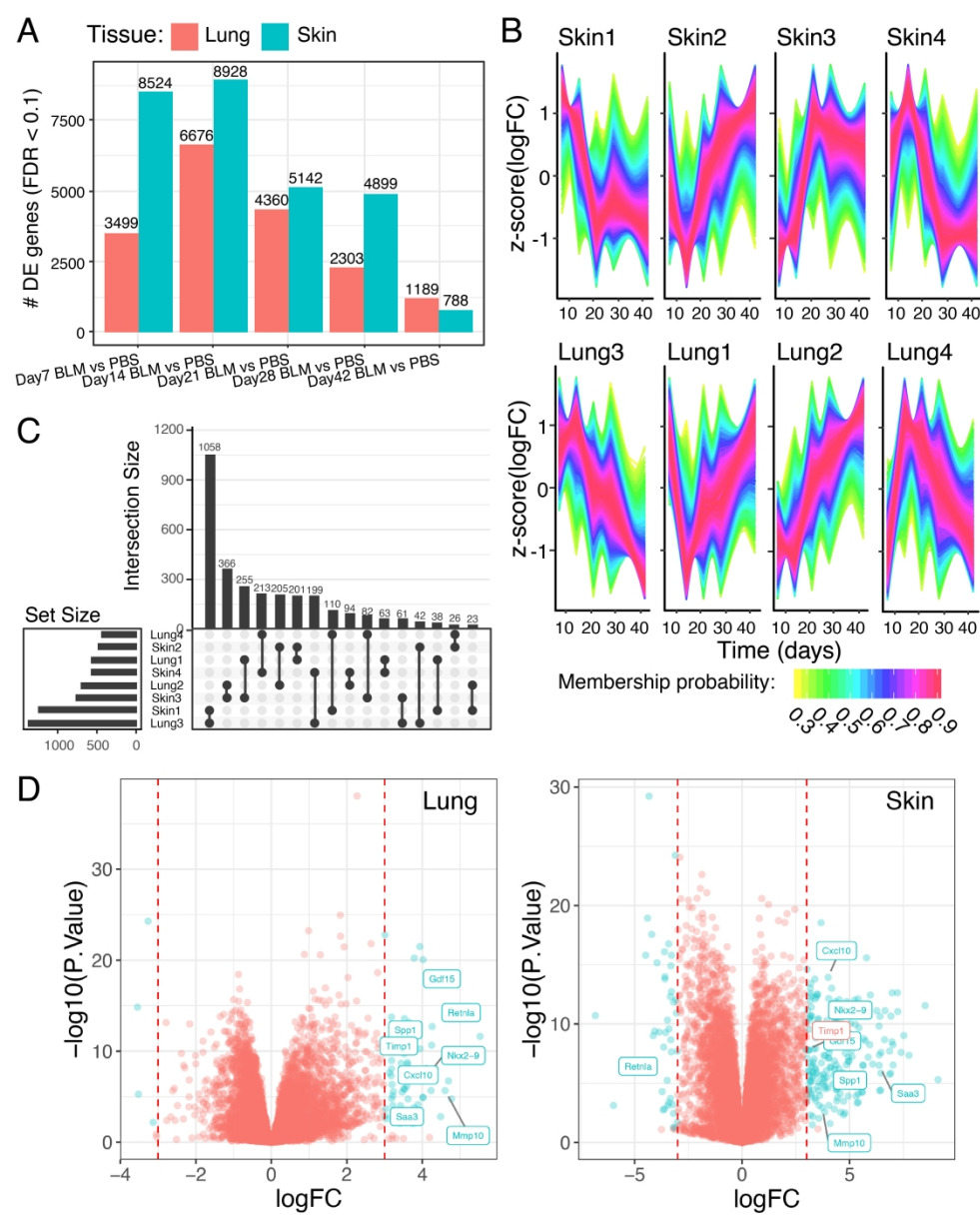


Figure 3: (A) Number of differentially expressed genes in lung and skin between bleomycin (BLM) and PBS treated mice. (B) Cluster-matched patterns of z-score normalized differential expression in skin (top) and lung (bottom). (C) UpSet plot showing the number of genes in each cluster (left) and magnitude of overlaps between clusters (top). (D) Volcano plots of differential expression in skin and lung, colored by FDR-corrected significance in skin and an absolute log-fold-change ≥ 3 , with shared genes labeled on the lung volcano plot.

200x247mm (600 x 600 DPI)

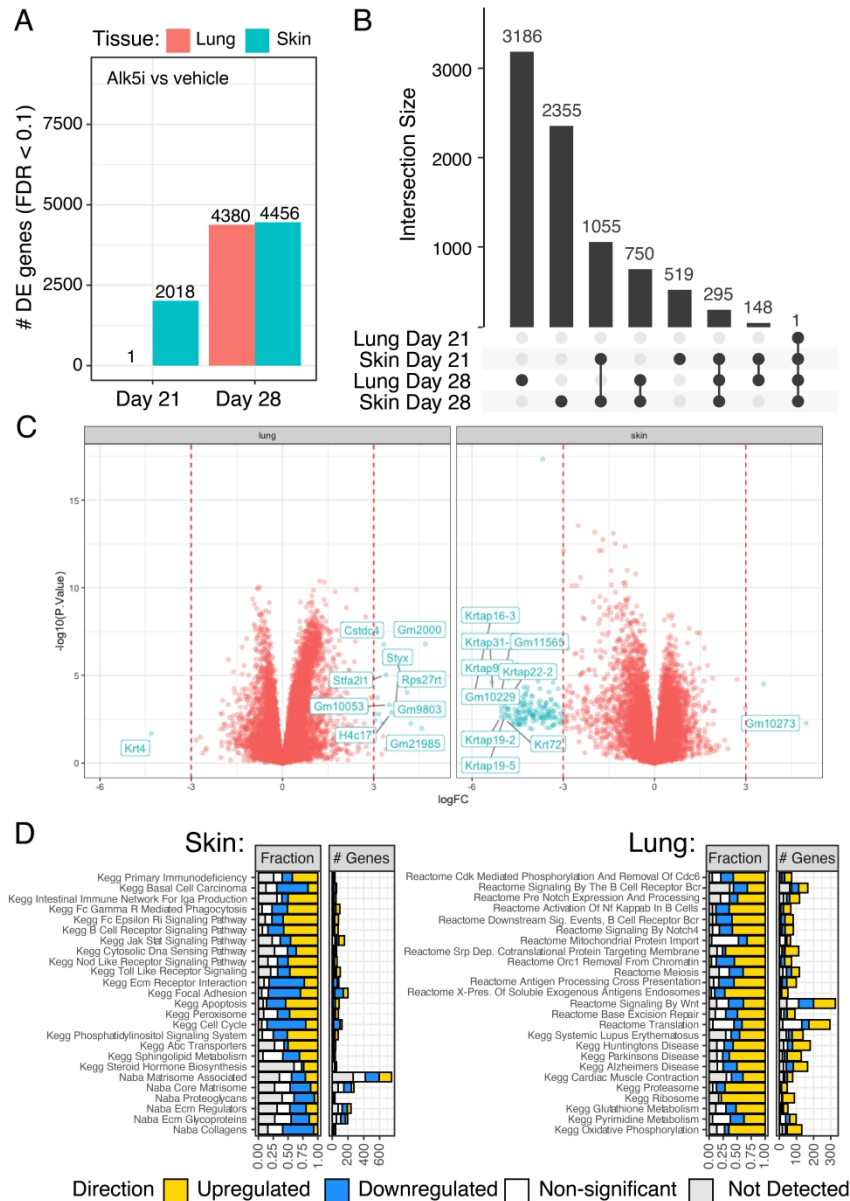


Figure 4: (A) Number of differentially expressed genes in lung and skin between ALK5 inhibitor treated and PBS treated mice. (B) UpSet plot showing the overlap of differentially expressed gene sets in the four time/tissue pairs for ALK5 inhibitor vs PBS treated mice. (C) Pathway enrichment UpDown plots showing the fraction and number of genes in each pathway upregulated/downregulated in the SB525334 arm compared to vehicle on day 28 for skin and lung.

199x283mm (600 x 600 DPI)

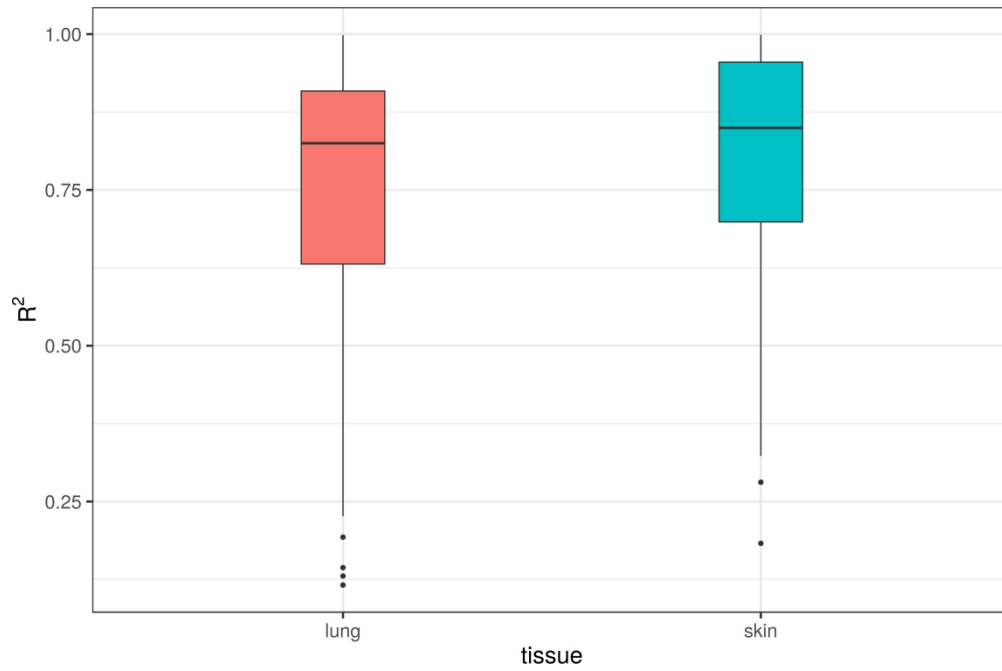


Figure 5: Boxplots of R² predictive power for elastic net models predicting inspiratory capacity trained on expression data from lung and skin.

148x97mm (600 x 600 DPI)

1
2
3
4
5
6
7
8
9
10
11
12
13
14
15
16
17
18
19
20
21
22
23
24
25
26
27
28
29
30
31
32
33
34
35
36
37
38
39
40
41
42
43
44
45
46
47
48
49
50
51
52
53
54
55
56
57
58
59
60